Supporting Information

Electronic structure regulation of halogen anions intercalated MgAl-LDH for highly selective photo-thermal oxidation of CH_4

Xiaoliang Sun,[a] Yanqi Xu,[a,b] Sha Bai,[a] Guihao Liu,[a] Tianyang Shen,[a] and Yu-Fei Song[a]*

[a]State Key Laboratory of Chemical Resource Engineering, Beijing University of Chemical Technology, Beijing 100029, P. R. China. E-mail: songyf@mail.buct.edu.cn;

[b]Key Laboratory of New Processing Technology for Nonferrous Metal & Materials, Ministry of Education, Collaborative Innovation Center for Exploration of Nonferrous Metal Deposits and Efficient Utilization of Resources, Guilin University of Technology, Guilin 541004, China

Table of Contents:

	condition, MgAl-F and MgAl-CO_3 under argon condition.
Figure S7.	The (a) XRD and (b) FTIR data for the MgAl-F after 5 cycle, (c) High-resolution Mg 1s and Al 2p XPS spectra of the MgAl-F sample after the reaction in reference to the fresh sample. (d) High-resolution O 1s and F 1s XPS spectra of the MgAl-F sample after the reaction in reference to the fresh sample.
Figure S8.	The chromatogram of MgAl-x after the reaction from GC-2014.
Figure S9.	(a) Optical power density of the high pressure 300 W Xenon lamp (Beijing Perfect Light Company, 240-2000 nm), the data was detected with PLS-MW2000 (Beijing Perfect Light Company), (b) the reaction temperature under the high pressure 300 W Xenon lamp (3455 $mW \cdot cm^{-2}$).
Figure S10.	(a) corresponding $(\alpha h\nu)^2$ versus photon energy plots, (b) VB-XPS data of MgAl-MgAl-x (x= F, Cl, Br, I).
Figure S11.	Mott-Schottky data of MgAl-x (x= CO_3, NO_3, F, Cl, Br, I).
Figure S12.	Electrochemical impedance spectra of MgAl-x (x= F, Cl, Br, I).
Figure S13.	(a) Mg 1s and (b) Al 2p XPS data of MgAl-x (x= F, Cl, Br, I).
Figure S14.	*In-situ* DRIFTS characterizations of (a) MgAl-F and (b) MgAl-I under CH_4 and H_2O flow with UV-vis irradiation.
Figure S15.	*In-situ* DRIFTS characterizations of MgAl-Cl under CH_4 and H_2O flow with (a) UV-vis irradiation and (b) UV-vis irradiation and 250°C.
Figure S16.	*In-situ* DRIFTS characterizations of MgAl-Br under CH_4 and H_2O flow with (a) UV-vis irradiation and (b) UV-vis irradiation and 250°C.
Figure S17.	The adsorption energy of MgAl-x for *CO and *CH_3
Table S2.	Total energy of several species for calculation of energy data of MgAl-x (x= F, Cl, Br, I).
Reference	

Experimental methods

1. Synthesis

MgAl-CO_3 was synthesized by the co-precipitation method.[1] MgAl-NO_3 was synthesized by the anions exchange method. 6.5 g MgAl-CO_3 was dispersed into 585 mL anhydrous methanol, stirring for 6 h at room temperature with N_2 protection. Then, 4 mL of concentrated nitric acid dissolved in 65 mL anhydrous methanol was added to the suspension, stirring for 6 h with N_2 protection. Then the slurry was filtered and washed five times with anhydrous methanol. The solid was then dried (65 °C)

MgAl-x (x= F, Cl, Br, I) was synthesized by suspending 500 mg MgAl-NO_3 in 48.5 mL 1.0 M aqueous alkali salt (NaF, NaCl, KBr, NaI) solutions and letting the rigorously vortexed nanopowder soak for 45 min.[2] Then the slurry was filtered and washed five times with decarbonated water. The solid was then dried (65 °C)

2. Characterization

XRD patterns were recorded by using a Bruker D8 diffractometer with Cu-Kα radiation (λ=1.5405 Å). The Fourier transform infrared (FT-IR) spectra were acquired on a NICOLET FT-IR spectrometer in a KBr tablet, scanning from 4000 to 400 cm^{-1} at room temperature. High-resolution transmission electron microscopy (HRTEM) images were performed on a JEOL JEM-2010 with an acceleration voltage of 200 kV. Room-temperature UV-vis diffuse reflectance spectroscopy (DRS) was recorded on a PerkinElmer Lambda 950 UV-vis-NIR spectrophotometer. X-ray photoelectron spectroscopy (XPS) measurements were explored with monochromatized Al K exciting X-radiation (PHI Quantera SXM). O K-edge X-ray absorption near-edge structure (XANES) measurements were performed at the 4B7B beamline of the Beijing Synchrotron Radiation Facility. The products of the photocatalytic reactions were analyzed by gas chromatography (Shimadzu GC 2014C, TCD detector, He as carrier gas). *In-situ* DRIFT was performed in a homemade in-situ reaction cell on BRUKER TENSOR II spectrometer.

2.1 Photocatalytic test

The photocatalytic performance of the MgAl-x (x= F, Cl, Br, I) and other comparative samples for methane conversion was tested at room temperature under full irradiation from a high pressure 300 W Xenon lamp (Beijing Perfect Light Company,240-2000 nm). The reactor was pumped to vacuum, followed by the introduction of 0.14 MPa of pure argon and 0.01 MPa methane (99.999%).

The gaseous product was analyzed by Shimadzu GC-2014 chromatography equipped with both FID and TCD detectors. The isotopic experiment was carried out under the same condition except using $^{13}CH_4$ (Linde Gas Comp. 99%) and gas chromatography-mass spectrometry (GC-MS, QP2020 equipped with Micropacked column), to check the products.

2.2 Productivity calculation

H_2 was detected by FID. CH_4, C_2H_6, and other alkanes were detected with TCD1. CO_2, CO, and CH_4 were detected with TCD2. All these species' peak areas were collect with standard gas (Beijing Star Standard Material Technology Co., Ltd.) peak area to calculate the productivity. Course CH_4 could be detected by FID and TCD, the peak area of CH_4 was used to correct the amount of all the species (CH_4, C_2H_6, CO_2, CO).

2.3 Spin-polarized and Hubbard corrected density functional theory calculations

The models of MgAl-x containing four different anions are constructed with Mg^{2+}/Al^{3+} ratio of 2/1. The parameters of the models are obtained by the X-ray crystallographic data of brucite: $P\bar{3}m1$ space group, $\alpha = \beta = 90°$, $\gamma = 120°$; the formulae and other lattice parameters (a, b, and c) are taken from the powder X-ray diffraction data of these LDHs (Tables S1).

The spin-polarized and Hubbard-corrected DFT calculations were carried out in the CASTEP code in Accelrys Materials Studio software package (Accelrys Software Inc., San Diego, CA).[3] The plane wave implementation[4] at the level of generalized gradient approximation (GGA) Perdew-Burke-Ernzerhof (PBE)[5] was used. The norm-conserving pseudopotential was used to describe the ionic core in calculating the Kohn-Sham equations.[6] The Broyden-Fletcher-Goldfarb-Shanno (BFGS) algorithm was employed in searching for the potential energy surface. The cutoff energy of 380 eV was set. The geometry optimization was based on the following points: (1) an energy tolerance of 5.0×10^{-5} eV per atom, (2) a maximum displacement tolerance of 0.005 Å, and (3) a maximum force tolerance of 0.01 eV/Å. When calculating the density of states, the Γ-point-centered k-point mesh for the Brillouin zone integration was 1 × 1 × 1 in the a-, b-, and c- directions.

Figures and Tables

Table S1. Details of the XRD data of MgAl-x (x= CO_3, NO_3, F, Cl, Br, I)

	2θ	c=$D_{(003)}$/nm	a=b/nm
MgAl-CO_3	**11.64**	**0.76**	**0.31**
MgAl-NO_3	**9.82**	**0.89**	**0.31**
MgAl-F	**11.68**	**0.75**	**0.31**
MgAl-Cl	**11.53**	**0.77**	**0.31**
MgAl-Br	**11.49**	**0.78**	**0.31**
MgAl-I	**11.10**	**0.80**	**0.31**

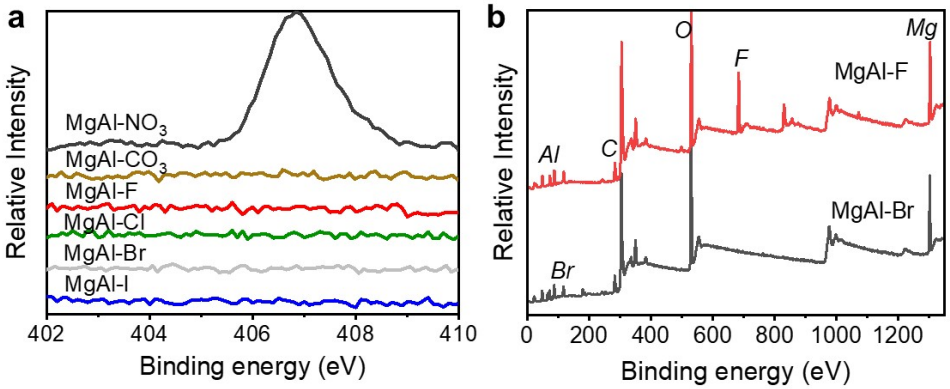

Figure S1. (a) The N 1s XPS data of the MgAl-x (x= CO_3, NO_3, F, Cl, Br, I), (b) the full XPS spectrum of MgAl-F and MgAl-Br.

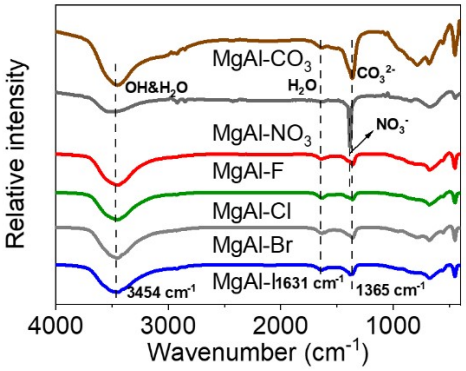

Figure S2. FTIR data of the MgAl-x (x= CO_3, NO_3, F, Cl, Br, I).

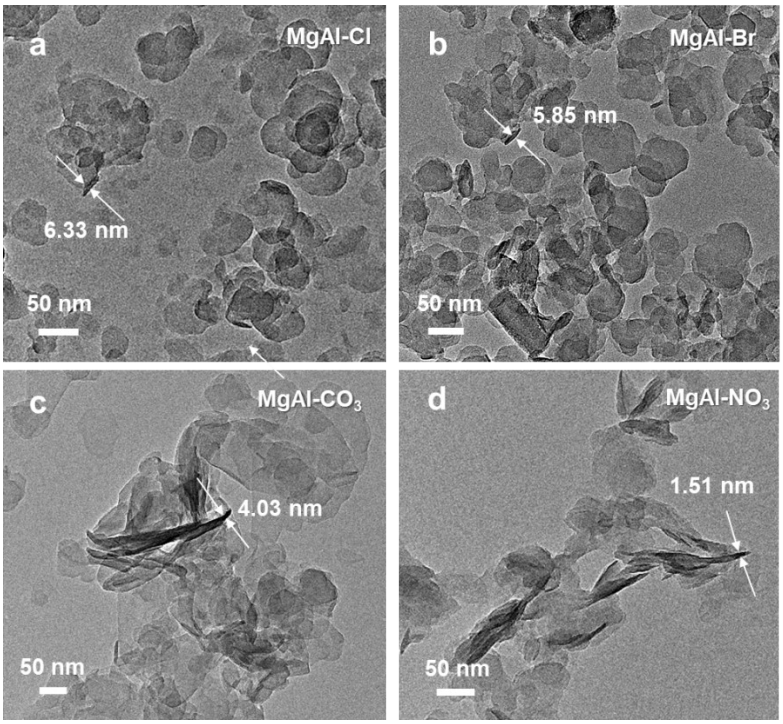

Figure S3. TEM of MgAl-x (x= CO_3, NO_3, Cl, Br,)

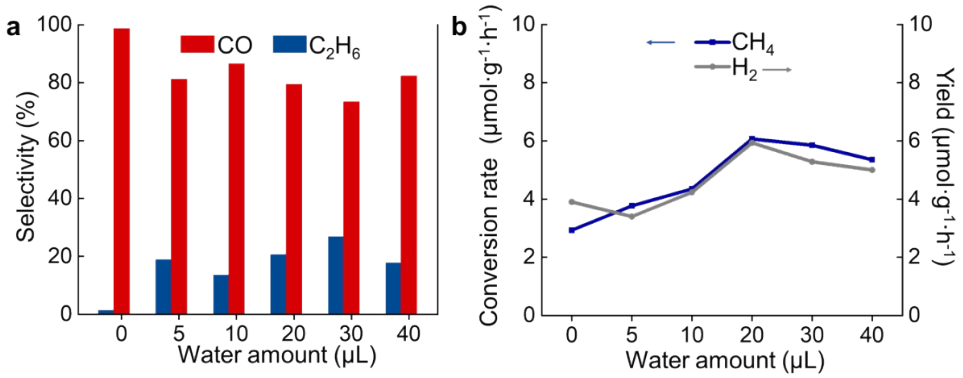

Figure S4. The performance of the MgAl-F at (a) different H_2O amount, Conditions: 20 mg cat, 0.14 MPa Ar+CH_4 (Ar:CH_4 =13:1), t=3 h, I=14 A, full Irradiation (3455 mW·cm^{-2})., (b) The H_2 yields of (a).

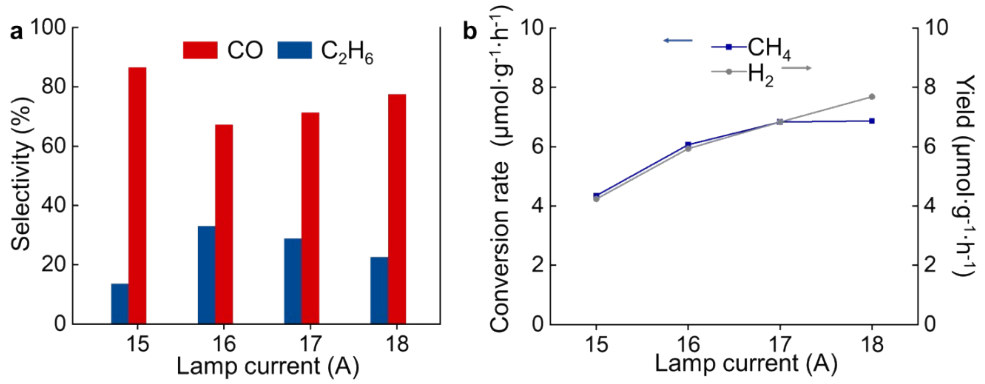

Figure S5. The performance of the MgAl-F at (a) different lamp current, Conditions: 20 mg Catalyst, 10 μL H_2O, 0.14 MPa Ar+CH_4 (Ar:CH_4 =13:1), t=3 h, full Irradiation. (b) The H_2 yields of (a).

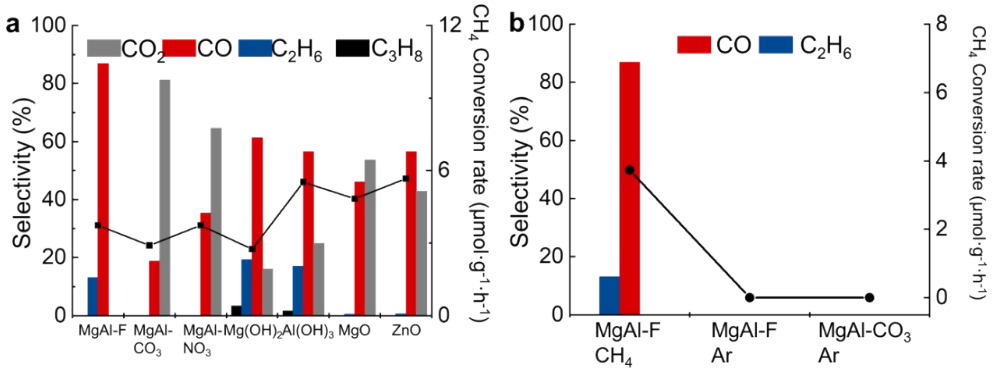

Figure S6. (a) Comparative test with several materials. Conditions: 20 mg Catalyst, 0.14 MPa Ar+CH_4 (Ar:CH_4 =13:1), 30 μL H_2O, t=3 h, full Irradiation (3455 mW·cm^{-2}). (b) The performance of the MgAl-F at CH_4 condition, MgAl-F and MgAl-CO_3 under argon condition.

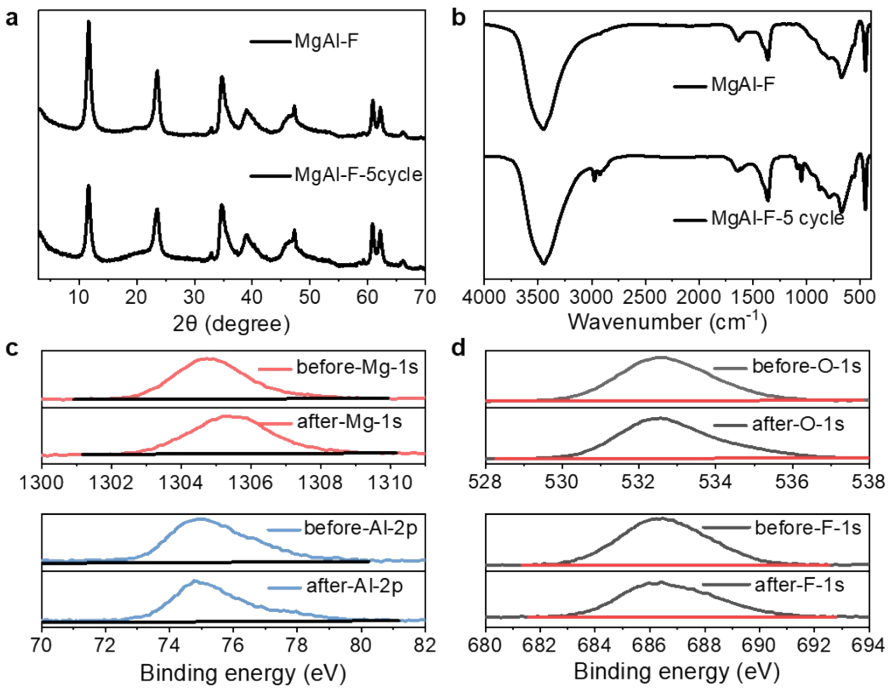

Figure S7. The (a) XRD and (b) FTIR data for the MgAl-F after 5 cycle, (c) the Mg 1s and Al 2p XPS spectra of the MgAl-F sample after the reaction in reference to the fresh sample. (d) High-resolution O 1s and F 1s XPS spectra of the MgAl-F sample after the reaction in reference to the fresh sample.

As shown in Figure S7c-d, right after the photocatalytic reaction, the binding energy of O in MgAl-F decrease and that of Mg increased, but the binding energy of Al and F were stable, indicating that the Mg and O were the key active sites of the reaction.

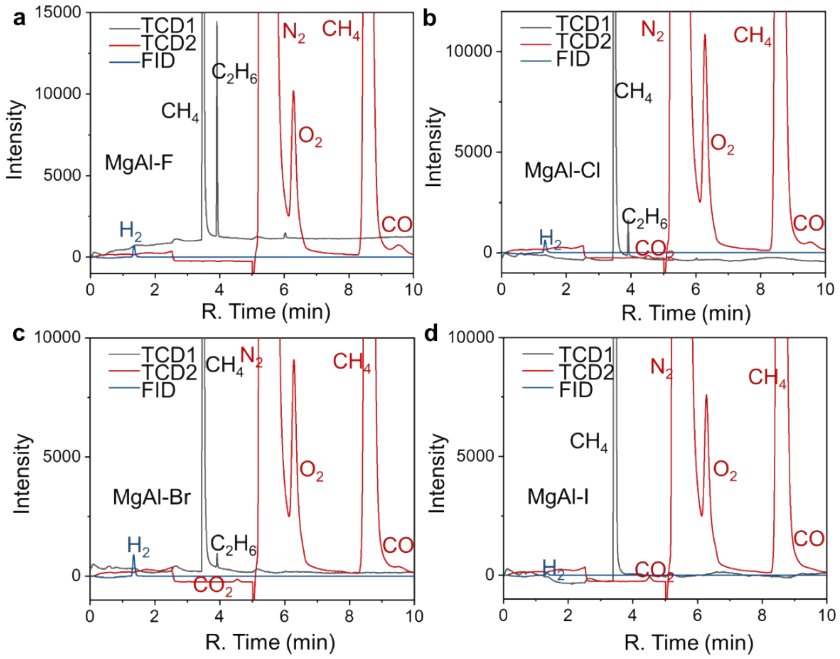

Figure S8. The chromatogram of MgAl-x after the reaction from GC-2014.

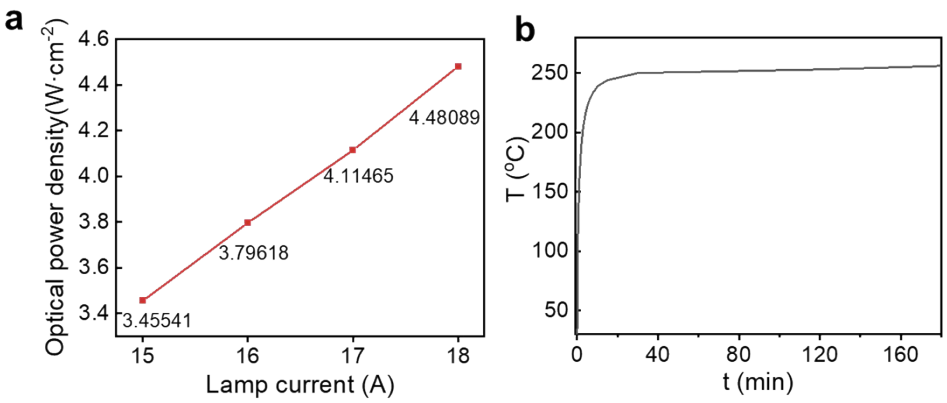

Figure S9. (a) Optical power density of the high pressure 300 W Xenon lamp (Beijing Perfect Light Company, 240-2000 nm), the data was detected with PLS-MW2000 (Beijing Perfect Light Company), (b) the reaction temperature under the high pressure 300 W Xenon lamp (3455 mW·cm^{-2}).

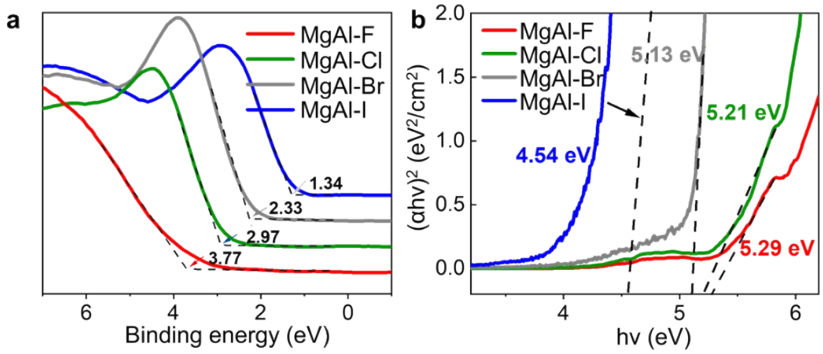

Figure S10. (a) corresponding $(\alpha h\nu)^2$ versus photon energy plots, (b) VB-XPS data of MgAl-x (x= F, Cl, Br, I).

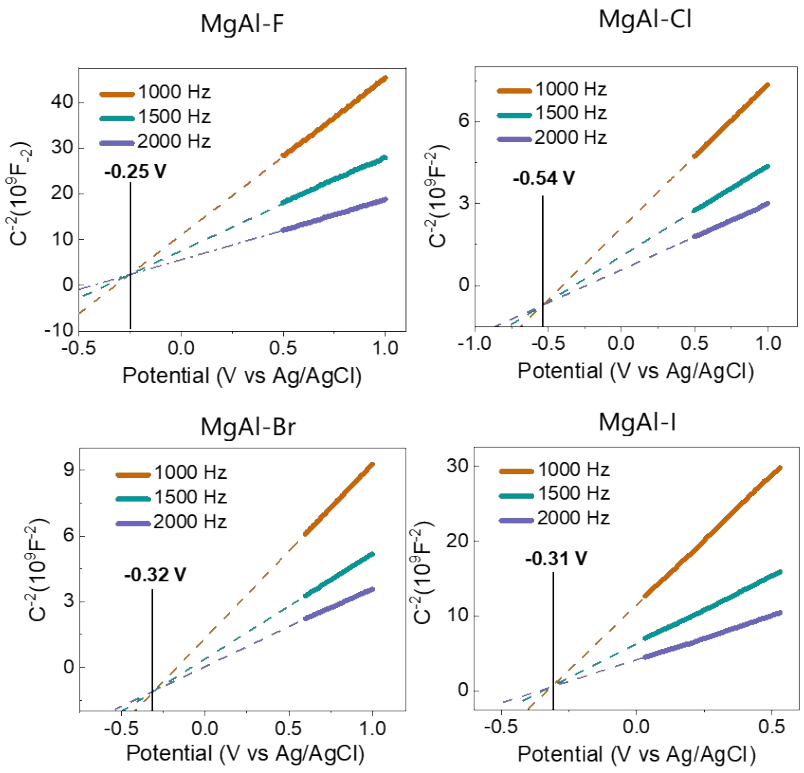

Figure S11. Mott-Schottky data of MgAl-x (x= F, Cl, Br, I).

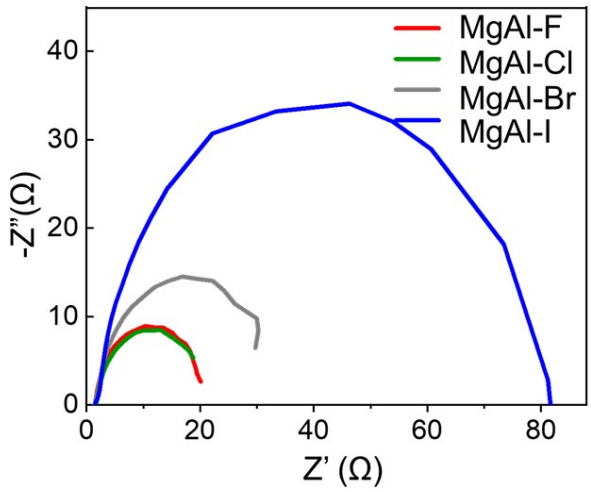

Figure S12. Electrochemical impedance spectra of MgAl-x (x= F, Cl, Br, I).

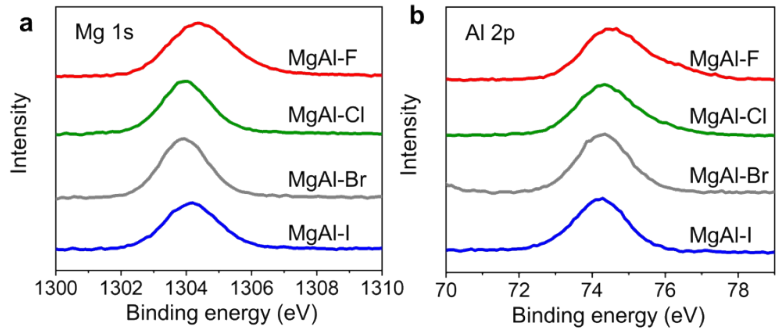

Figure S13. (a) Mg 1s and (b) Al 2p XPS data of MgAl-x (x= F, Cl, Br, I).

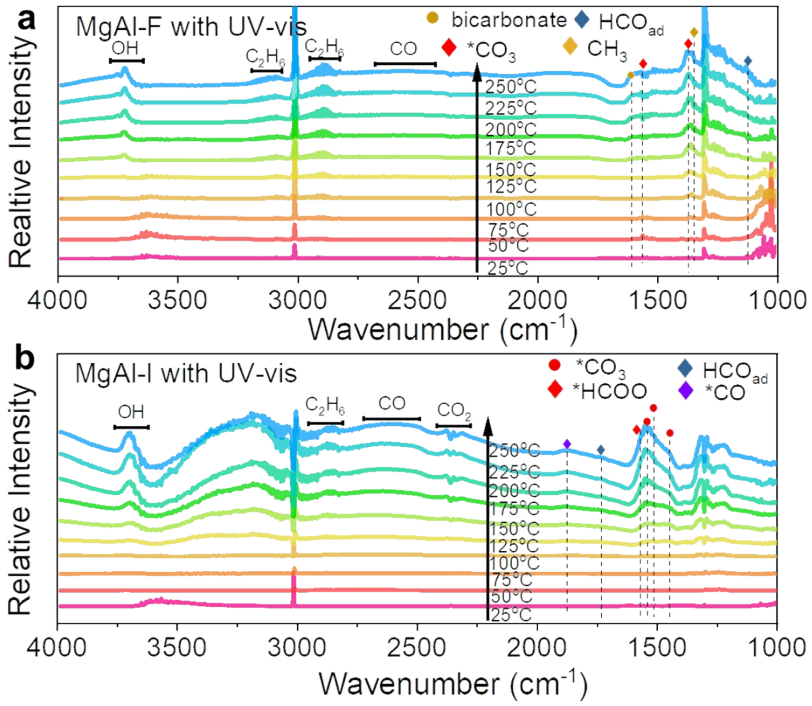

Figure S14. *In-situ* DRIFTS characterizations of (a) MgAl-F and (b) MgAl-I under CH_4 and H_2O flow with UV-vis irradiation.

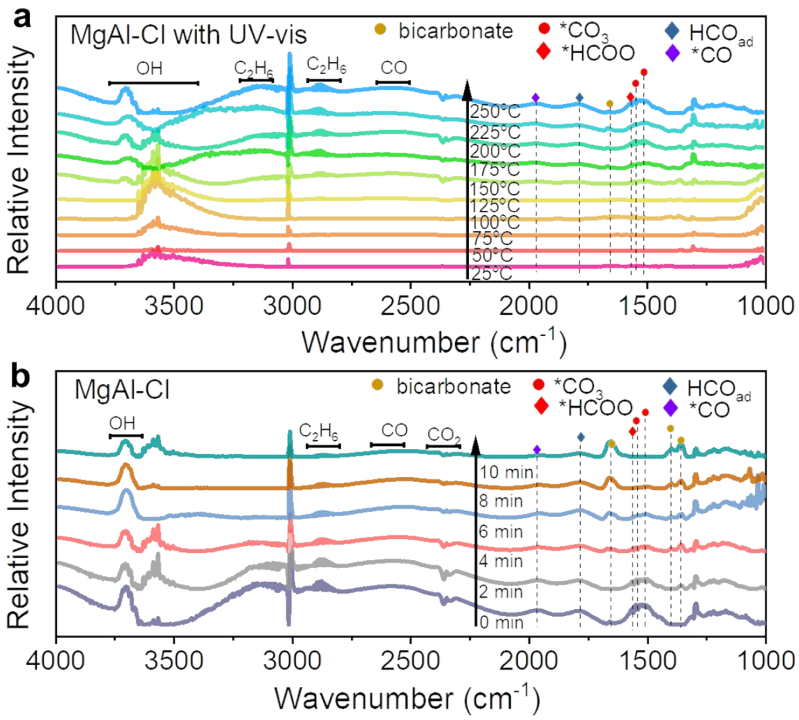

Figure S15. *In-situ* DRIFTS characterizations of MgAl-Cl under CH_4 and H_2O flow with (a) UV-vis irradiation and (b) UV-vis irradiation and 250°C.

For the MgAl-Cl, with the reaction time increasing, the peak of *HCOO disappears, and two strong peak at 1663 and 1364 cm^{-1} appear, indicating that *HCOO converts to $*HCO_3$ quickly when the reaction gets stable.

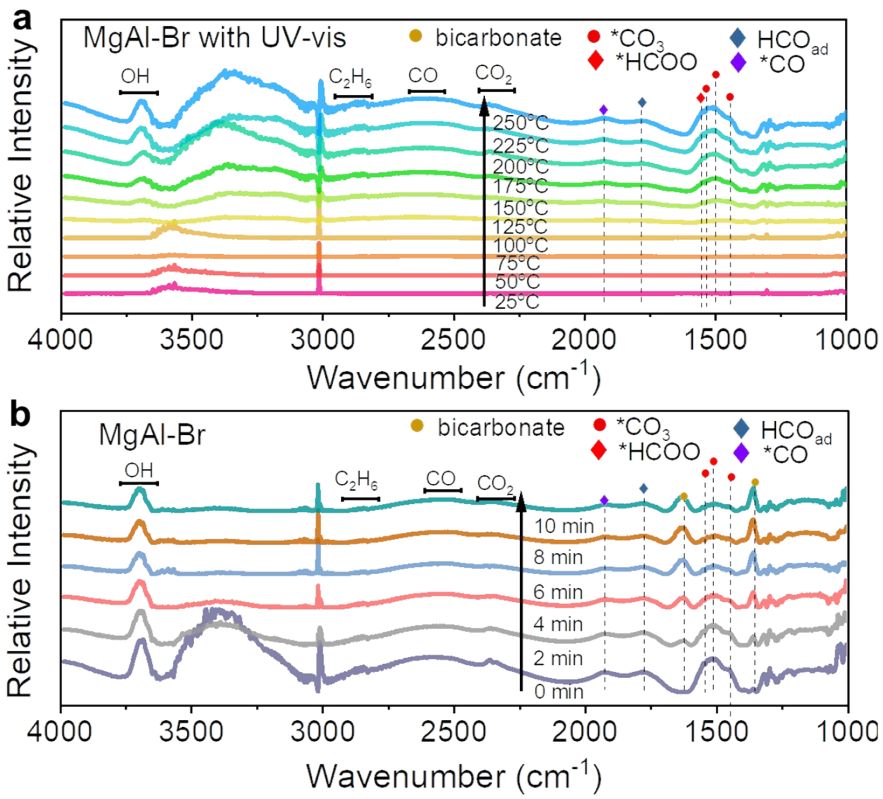

Figure S16. *In-situ* DRIFTS characterizations of MgAl-Br under CH_4 and H_2O flow with (a) UV-vis irradiation and (b) UV-vis irradiation and 250°C.

For the MgAl-Br, with the reaction time increasing, the peak intensity of $*CO_3$ decreases and get stable in 8 min. Like MgAl-Cl, the content of $*CO_3$ increases.

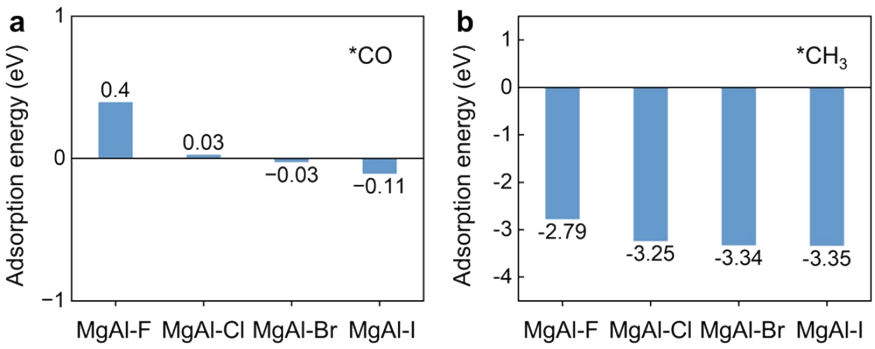

Figure S17. The adsorption energy of MgAl-x for *CO and $*CH_3$.

Table S2. Total energy of several species for calculation of energy data of MgAl-x (x= F, Cl, Br, I).

	Total energy(eV)

F-CH_3-H-O	-62192.40555839
F-CH_2-H-O	-62174.17433596
F-CO-H	-62580.05812686
F-HOCO-H	-63035.00725878
F-perfect	-61986.31991365
Cl-CH_3-H-O	-60062.54813505
Cl-CH_2-H-O	-60044.39444223
Cl-CO-H	-60450.02892140
Cl-HOCO-H	-60904.9889214
Cl-perfect	-59855.98896135
Br-CH_3-H-O	-60428.43063886
Br-CH_2-H-O	-60410.25033177
Br-CO-H	-60815.87652559
Br-HOCO-H	-61271.07590023
Br-perfect	-60221.78449987
I-CH_3-H-O	-63417.68581780
I-CH_2-H-O	-63399.65390586
I-CO-H	-63805.23276590
I-HOCO-H	-64260.57237087
I-perfect	-63211.04729972
CH_3	-203.3027183170
CO	-594.0689080342

Adsorption energy calculation: $E_{ad} = E_{total}-E_{X\text{-}perfect}-E_{adsorp\ molecule}$

Reference

[1] Teramura, K.; Iguchi, S.; Mizuno, Y.; Shishido, T.; Tanaka, T., Photocatalytic Conversion of CO_2 in Water over Layered Double Hydroxides. *Angew. Chem. Int. Ed.* **2012,** *51* (32), 8008-11.

[2] Khodakov, A. Y.; Chu, W.; Fongarland, P., Advances in the Development of Novel Cobalt Fischer−Tropsch Catalysts for Synthesis of Long-Chain Hydrocarbons and Clean Fuels. *Chem. Rev.* **2007,** *107*, 1692-1744.

[3] Segall, M. D.; Lindan, P. J. D.; Probert, M.; Pickard, C. J.; Hasnip, P.; Clark, S. J.; Payne, M., First-Principles Simulation: Ideas, Illustrations and The CASTEP Code. *J. Phys. Condens. Matter* **2002,** *14*, 2717-2744.

[4] Payne, M. C.; Teter, M. P.; Allan, D. C.; Arias, T. A.; Joannopoulos, J. D., Iterative Minimization Techniques Forab Initiototal-Energy Calculations: Molecular Dynamics and Conjugate Gradients. *Rev. Modern Phys.* **1992,** *64* (4), 1045-1097.

[5] Perdew, J. P.; Burke, K.; Ernzerhof, M., Generalized Gradient Approximation Made Simple. *Phys. Rev. Lett.* **1996,** *77*, 3865-3868.

[6] Colmenero, F.; Cobos, J.; Timon, V., Periodic Density Functional Theory Study of the Structure, Raman Spectrum, and Mechanical Properties of Schoepite Mineral. *Inorg. Chem.* **2018,** *57* (8), 4470-4481.